Hindawi Publishing Corporation
Journal of Nanomaterials
Volume 2013, Article ID 621378, 6 pages
http://dx.doi.org/10.1155/2013/621378

Research Article

Influence of Sodium Dodecyl Sulfonate on the Formation of ZnO Nanorods from ε-$Zn(OH)_2$

Jing Wang, Chengxiang Liu, and Lan Xiang

Department of Chemical Engineering, Tsinghua University, Beijing 10084, China

Correspondence should be addressed to Lan Xiang; xianglan@mail.tsinghua.edu.cn

Received 28 December 2012; Accepted 18 April 2013

Academic Editor: Yunpeng Yin

The influence of sodium dodecyl sulfonate (SDSN) on the formation of ZnO nanorods from ε-$Zn(OH)_2$ was investigated in this paper. The ε-$Zn(OH)_2$ precursor was prepared at room temperature using $ZnSO_4$ and NaOH as the reactants and then converted to ZnO nanorods after aging at 80°C in NaOH solution containing a minor amount of sodium dodecyl sulfonate (SDSN). The experimental results and the molecular simulation revealed that the influence of SDSN on the formation of ZnO from ε-$Zn(OH)_2$ should be attributed to the adsorption of SDSN on ε-$Zn(OH)_2$ surfaces, which inhibited the dissolution of ε-$Zn(OH)_2$ in NaOH solution, leading to the formation of the ZnO nanorods with a diameter of 50–200 nm, a length of 3.0–15.0 μm, and an aspect ratio of 30–100.

1. Introduction

As a wide band gap semiconductor with an excitation binding energy of 60 meV at room temperature, one-dimensional (1D) ZnO is a promising candidate for many applications such as UV lasers, field emission, solar cells, and piezoelectric devices [1–4]. Extensive work has been carried out on the morphology control of 1D ZnO nanostructures since their performances are strongly shape or size dependent.

The wet chemical route is one of the promising approaches to synthesize 1D ZnO nanostructures owing to the moderate condition and the easy control of the products. The surfactants are often used in the wet chemical route to adjust the morphology of 1D ZnO. It was reported that ZnO nanowire arrays with a diameter of 20~500 nm and a length of 1~40 μm were synthesized after aging the solutions containing 0.0001~0.1 mol·L^{-1} zinc nitrate hexahydrate and 0.0001~0.1 mol·L^{-1} hexamethylene tetramine (HMTA) at 60~95°C for 2.0~48.0 h [5–7], and the presence of 0.008~0.01 mol·L^{-1} polyethylenimine (PEI) could inhibit the lateral growth of ZnO [8, 9]. The ZnO nanorods with an average diameter of 50 nm and an aspect ratio of 30–40 were synthesized at 180°C from the solution containing 0.05 mol·L^{-1} $Zn(NO_3)_2$, 1.0 mol·L^{-1} NaOH, and ethylenediamine ($[Zn^{2+}]:[EDA]$ = 1:50~60) [10]. The poor efficiency derived from the dilute solutions restricted the further applications of the above methods, and, moreover, the detailed mechanisms about the influence of surfactants on the formation of 1D ZnO were still unclear.

Recently, the formation of 1D ZnO from ε-$Zn(OH)_2$ precursor has attracted much attention owing to the high efficiency of the processes [11–19]. For example, McBride et al. [15] reported the formation of ZnO microrods with an average diameter of 1.0 μm and an aspect ratio of 6~10 in an aqueous solution containing 0.025 mol·L^{-1} $Zn(NO_3)_2$ and 0.375 mol·L^{-1} NaOH. Xie et al. [18, 19] suggested an SDS-assisted method to produce needle-like ZnO with a diameter of 450~550 nm, a length of 11~16 μm, and an aspect ratio of 20–30. It was noticed that, up to now, the aspect ratios of the 1D ZnO obtained from ε-$Zn(OH)_2$ precursor were usually smaller than 30, and it is still a challenge to synthesize 1D ZnO with high aspect ratios.

In this paper, a facile SDSN-assisted method was developed to synthesize the ZnO nanorods with an aspect ratio of 30–100 from ε-$Zn(OH)_2$ precursor. The influence of SDSN on the conversion of ε-$Zn(OH)_2$ to ZnO nanorods was investigated experimentally, and the detailed mechanism was revealed by the molecular simulation method.

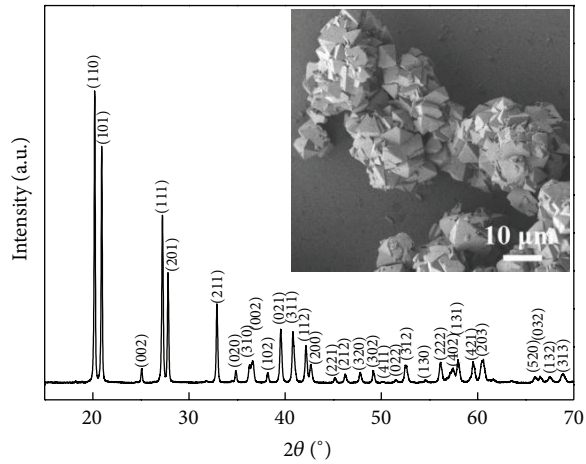

Figure 1: SEM image and XRD pattern of ε-$Zn(OH)_2$ precursor formed at room temperature.

2. Experimental

2.1. Synthesis. In a typical procedure, 2.0 mol·L^{-1} $ZnSO_4$ was added dropwise (5 mL·min^{-1}) into 4.0 mol·L^{-1} NaOH at 25°C under stirring (300 r·min^{-1}) until the molar ratio of Zn^{2+} : OH^- reached up to 1 : 2. The slurry was kept stirring for 10 min; then, the precipitate was filtrated, washed with deionized water, and mixed with SDSN, NaOH, and deionized water to produce a slurry containing 0.02 mol·L^{-1} SDSN, 1.0 mol·L^{-1} NaOH and 3.0 wt% ε-$Zn(OH)_2$. The 40.0 mL slurry was transferred into a 70 mL Teflon-lined stainless steel autoclave and sealed and kept thermostatic at 80°C for 4.0 h. Then, the product was filtrated, washed with deionized water for three times, and dried at 60°C for 12.0 h.

2.2. Analysis. The composition and structure of the samples were identified by an X-ray powder diffractometer (XRD, Bruker-AXS D8 Advance, Germany) using CuKα radiation (λ = 0.154178 nm). The morphology of the samples was examined by a field emission scanning electron microscopy (FESEM, JSM 7401F, JEOL, Japan) and a high resolution transmission electron microscopy (HRTEM, JEM-2010, JEOL, Japan). The functional groups of the samples were examined by a Fourier transform infrared spectrometer (FT-IR, Nexus, Nicolet, USA). The concentration of soluble Zn(II) was analyzed by the EDTA titration method. To get the molar ratio of ZnO in the solid products, 0.12 g sample was dissolved in 10 mL of 1 mol·L^{-1} hydrochloric acid and then buffered to pH 5-6 with an ammonia-ammonium chloride buffer, and the total amount of zinc was analyzed by EDTA titration. The molar ratio of ZnO could be calculated as the samples contained only ε-$Zn(OH)_2$ and ZnO.

2.3. Molecular Simulation Methods. Materials studio 4.3 software was used for simulation. The simulation was performed by the molecular mechanics (MM) and the molecular dynamics (MD) methods, using the Discover module and the Compass force field [20]. The Smart Minimizer was adapted for the minimization.

Based on the morphology of ε-$Zn(OH)_2$ deduced by BFDH method, (011), (101), (110), and (002) planes of ε-$Zn(OH)_2$ were chosen for molecular simulation. The planes containing 5 depths were cleaved and optimized using MM simulation to get the initial stable surfaces of ε-$Zn(OH)_2$. MM simulation was also performed to optimize the SDSN molecule.

The SDSN molecule was randomly located on the chosen planes with a vacuum slab of 3 nm. Then, the molecular dynamics simulations were performed in the NVT ensemble at 298 K using the Nosé thermostat [21]. The total simulation time is 100 ps, including 50 ps for removing the unfavorable local minima and 50 ps for the date analysis. The movement and the trajectory of the atoms were saved every 1 ps. The interaction energy is calculated according to the following equation: $E_{\text{Interaction}} = E_{\text{total}} - (E_{\text{surface}} + E_{\text{SDSN}})$, where E_{total} is the total energy of the surface and the SDSN molecule, E_{surface} is the energy of the surface without the SDSN molecule, and E_{SDSN} is the energy of the SDSN molecule without the surface.

3. Results and Discussion

Figure 1 shows the SEM image and XRD pattern of the precursor formed at room temperature. All of the diffraction peaks can be indexed as those of the orthorhombic ε-$Zn(OH)_2$ (JCPDS 38-0385). The ε-Zn $(OH)_2$ precursor was composed of agglomerated octahedral particles with a primary particle size of 5–7 μm.

The influence of SDSN on the morphology and XRD patterns of the products formed at 80°C is shown in Figure 2. The ZnO submicron rods with a diameter of 100–500 nm and a length of 1.0–5.0 μm, and the needle-like ZnO nanorods with a diameter of 50–200 nm and a length of 3.0–15.0 μm were prepared in the absence and presence of SDSN, respectively. The SAED pattern in Figure 2(b) revealed that the preferential orientation of the ZnO nanorods was along (001). The XRD patterns in Figure 2(c) indicated that the presence of SDSN led to the increase of the intensity ratios

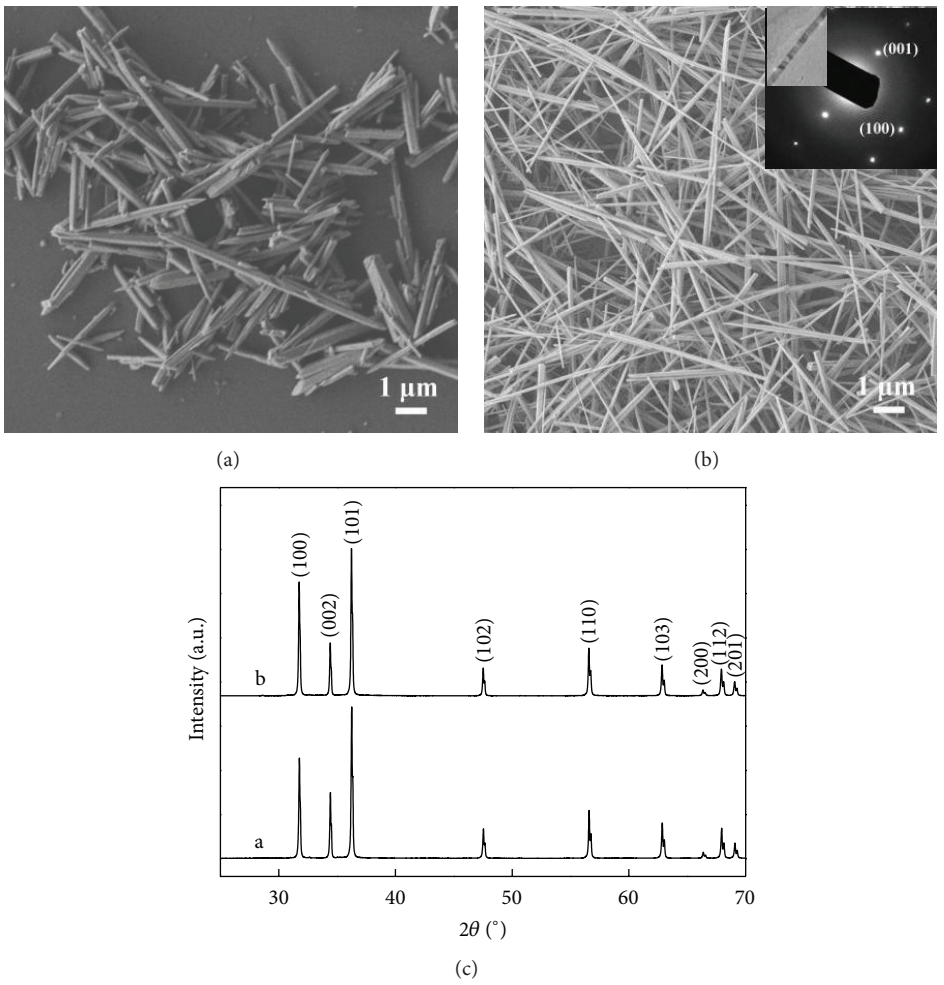

Figure 2: SEM images (a, b) and XRD patterns (c) of the products obtained from ε-$Zn(OH)_2$ SDSN ($mol \cdot L^{-1}$): a-0, b-0.02 $mol \cdot L^{-1}$.

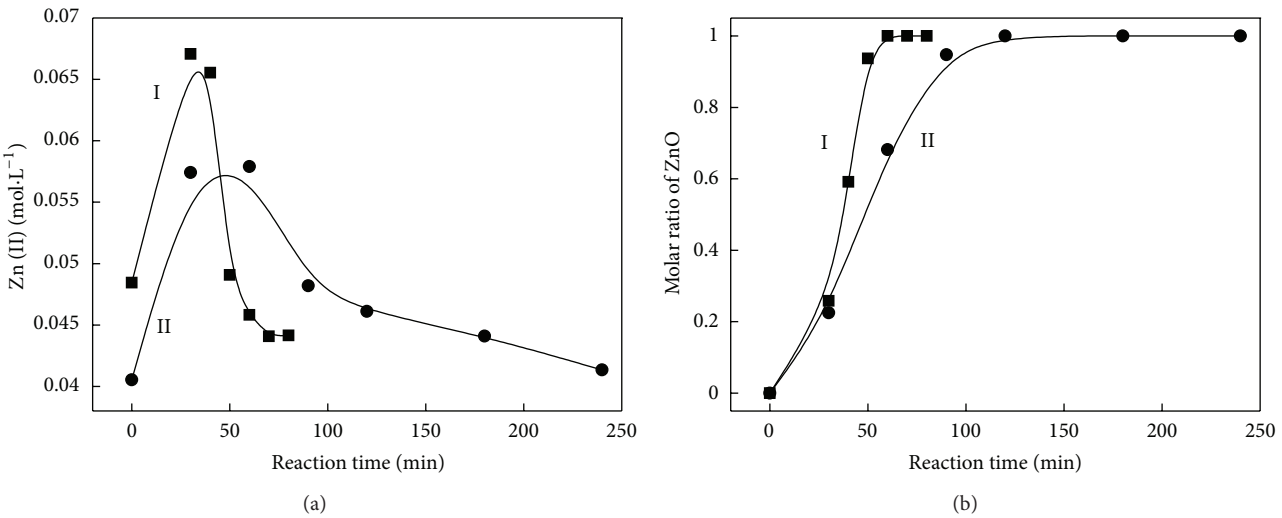

Figure 3: Variation of soluble Zn(II) (a) and molar ratio of ZnO in the products (b) with reaction time; SDSN ($mol \cdot L^{-1}$): I-0, II-0.02 $mol \cdot L^{-1}$.

Table 1: Interaction energies between SDSN and ε-$Zn(OH)_2$ planes ($kJ \cdot mol^{-1}$).

Plane	E_{total}	$E_{surface}$	E_{SDSN}	$E_{interaction}$	E_{vdw}	E_{coul}
(011)	259802.6	260905.7	128.89	−1231.98	48.24	−1280.22
(101)	577146.7	578236.5	234.46	−1324.28	81.55	−1405.83
(110)	545782.5	547542.5	229.38	−1989.36	72.60	−2061.96
(002)	498933.7	500393.1	44.35	−1503.70	79.85	−1583.55

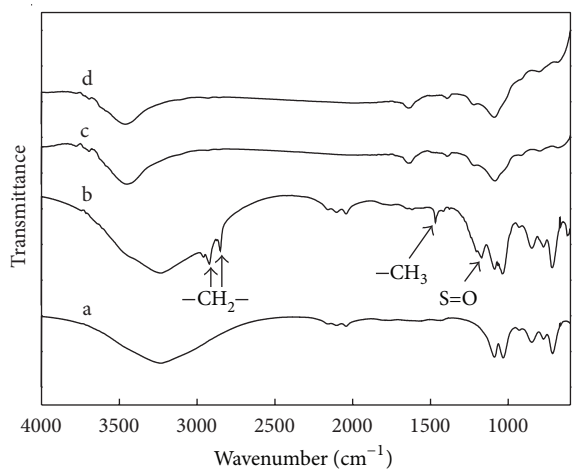

Figure 4: FT-IR spectra of ε-$Zn(OH)_2$ (a, b) and ZnO (c, d) SDSN ($mol \cdot L^{-1}$): a, c-0; b, d-0.02 $mol \cdot L^{-1}$.

of (100) to (002) from 1.52 to 2.14 owing to the enhanced preferential growth along (001). The above results showed that the presence of SDSN favored the formation of the ZnO nanorods with high aspect ratios. In addition, it was also found that the average aspect ratio of the ZnO nanorods increased gradually as the concentration of SDSN increased from 0 to 0.02 $mol \cdot L^{-1}$, whereas the morphology of the ZnO nanorods remained unchanged in the case of SDSN concentration >0.02 $mol \cdot L^{-1}$.

Figure 3 shows the variation of the soluble Zn(II) and the molar ratio of ZnO in the products with reaction time. The gradually increase of the soluble Zn(II) at the initial stage in Figure 3(a) revealed the faster dissolution of ε-$Zn(OH)_2$ than the precipitation of ZnO, while the decrease of the soluble Zn(II) at the later time should be attributed to the quicker precipitation of ZnO than the dissolution of ε-$Zn(OH)_2$. The change tendency of the soluble Zn(II) with reaction time indicated that the conversion of ε-$Zn(OH)_2$ to ZnO may proceed mainly via the dissolution-precipitation route, the ε-$Zn(OH)_2$ acted as a "reservoir," and the gradual release of soluble Zn(II) favored the 1D growth of ZnO nanorods. The data in Figures 3(a) and 3(b) also showed that the presence of SDSN led to the decrease of the maximum soluble Zn(II) concentration and the prolongation of the reaction time for the complete conversion of ε-$Zn(OH)_2$ to ZnO. The slow release of soluble Zn(II) from ε-$Zn(OH)_2$ in the presence of SDSN favored the 1D anisotropic growth of the ZnO, leading to the formation of ZnO nanorods with high aspect ratios.

The influence of SDSN on the dissolution of ε-$Zn(OH)_2$ may be connected with the interaction between SDSN and ε-$Zn(OH)_2$. Figure 4 shows the FT-IR spectra of ε-$Zn(OH)_2$ and ZnO formed in the absence and presence of SDSN. The ε-$Zn(OH)_2$ samples were prepared from the initial ε-$Zn(OH)_2$ slurries without aging, and the ZnO samples were obtained by aging of the ε-$Zn(OH)_2$ slurries at 80°C for 4.0 h. Compared with curve a, some new peaks occurred in curve b: the peak at 1170 cm^{-1} (the stretching vibration of S=O) and 1467 cm^{-1} (the stretching vibration of $-CH_3$) and the peaks at 2852 cm^{-1} and 2922 cm^{-1} (the stretching vibrations of $-CH_2-$), which confirmed the adsorption of SDSN on ε-$Zn(OH)_2$ surfaces. Meanwhile, the similar spectra of curve c and curve d indicated that SDSN was difficult to be adsorbed on ZnO surfaces. The detailed adsorption behavior of SDSN on ε-$Zn(OH)_2$ surfaces was investigated further by molecular simulation method.

Table 1 shows the interaction energies between the cleaved ε-$Zn(OH)_2$ planes and SDSN. The negative interaction energy values between SDSN and ε-$Zn(OH)_2$ indicated that SDSN was liable to be absorbed on ε-$Zn(OH)_2$ surfaces and the interaction energies were mainly attributed to the coulomb interaction. Figure 5 shows the detailed equilibrium conformations of SDSN on ε-$Zn(OH)_2$ surfaces. The sulfonate group ($-OSO_2^-$) in SDSN tended to attach to the ε-$Zn(OH)_2$ surfaces in the equilibrium adsorption states. Meanwhile, the interaction between SDSN and ZnO surfaces was also studied with the similar molecular simulation method. As the preferential orientation of the nanorods was along (001), the (001) plane and the (100) plane were chosen for the simulation study. The calculated interaction energies between SDSN and ZnO (001) and (100) planes were −5.1 $kJ \cdot mol^{-1}$ and 189.7 $kJ \cdot mol^{-1}$, indicating that SDSN was difficult to be absorbed on ZnO (100) surface while could be absorbed on (001) surface. According to the previous studies [22, 23], the adsorption of small molecules on (001) surface would inhibit the anisotropic growth of ZnO; thus, the promoted 1D growth of ZnO in the present of SDSN could not be reasonable explained by the adsorption of SDSN on ZnO.

4. Conclusions

The influence of SDSN on the formation of ZnO nanorods from ε-$Zn(OH)_2$ was investigated in this paper. The experimental results showed that the dissolution of ε-$Zn(OH)_2$ was inhibited by the adsorption of SDSN. The slow release of soluble Zn(II) from ε-$Zn(OH)_2$ in the presence of SDSN favored the anisotropic growth of ZnO, leading to the formation of the

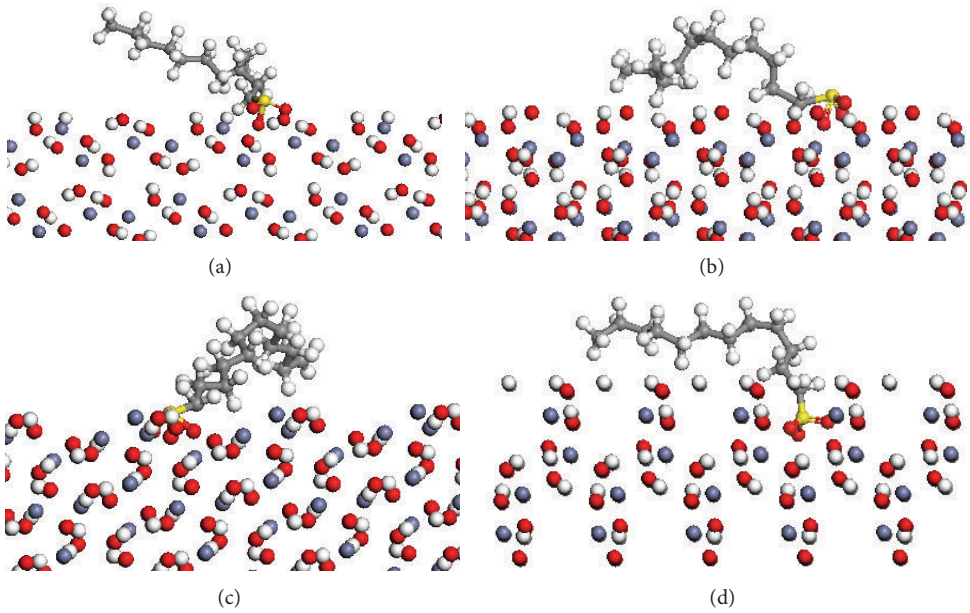

FIGURE 5: Snapshots of the equilibrium conformations of SDSN on ε-$Zn(OH)_2$ planes. Planes: (a): (011), (b): (101), (c): (110), and (d): (002). Blue circle: Zn, red circle: O, yellow circle: S, white circle: H, and gray circle: C.

ZnO nanorods with a diameter of 50–200 nm, a length of 3.0–15.0 μm, and an aspect ratio of 30–100. Molecular simulation results indicated that SDSN was liable to be adsorbed on ε-$Zn(OH)_2$ surfaces but difficult to be absorbed on ZnO (100) surface.

Acknowledgment

This work was supported by the National Natural Science Foundation of China (no. 51174125 and no. 51234003).

References

[1] M. H. Huang, S. Mao, H. Feick et al., "Room-temperature ultraviolet nanowire nanolasers," *Science*, vol. 292, no. 5523, pp. 1897–1899, 2001.

[2] Y. H. Huang, Y. Zhahg, L. Liu, S. S. Fan, Y. Wei, and J. He, "Controlled synthesis and field emission properties of ZnO nanostructures with different morphologies," *Journal of Nanoscience and Nanotechnology*, vol. 6, no. 3, pp. 787–790, 2006.

[3] M. Law, L. E. Greene, J. C. Johnson, R. Saykally, and P. Yang, "Nanowire dye-sensitized solar cells," *Nature Materials*, vol. 4, no. 6, pp. 455–459, 2005.

[4] X. Wang, J. Song, J. Liu, and L. W. Zhong, "Direct-current nanogenerator driven by ultrasonic waves," *Science*, vol. 316, no. 5821, pp. 102–105, 2007.

[5] J. Qiu, X. Li, W. He et al., "The growth mechanism and optical properties of ultralong ZnO nanorod arrays with a high aspect ratio by a preheating hydrothermal method," *Nanotechnology*, vol. 20, no. 15, Article ID 155603, 2009.

[6] L. Vayssieres, "Growth of arrayed nanorods and nanowires of ZnO from aqueous solutions," *Advanced Materials*, vol. 15, no. 5, pp. 464–466, 2003.

[7] C. Xu, P. Shin, L. Cao, and D. Gao, "Preferential growth of long ZnO nanowire array and its application in dye-sensitized solar cells," *Journal of Physical Chemistry C*, vol. 114, no. 1, pp. 125–129, 2010.

[8] J. Qiu, X. Li, F. Zhuge et al., "Solution-derived 40νm vertically aligned ZnO nanowire arrays as photoelectrodes in dye-sensitized solar cells," *Nanotechnology*, vol. 21, no. 19, Article ID 195602, 2010.

[9] W. Wu, G. Hu, S. Cui, Y. Zhou, and H. Wu, "Epitaxy of vertical ZnO nanorod arrays on highly (001)-oriented ZnO seed monolayer by a hydrothermal route," *Crystal Growth and Design*, vol. 8, no. 11, pp. 4014–4020, 2008.

[10] B. Liu and H. C. Zeng, "Hydrothermal synthesis of ZnO nanorods in the diameter regime of 50 nm," *Journal of the American Chemical Society*, vol. 125, no. 15, pp. 4430–4431, 2003.

[11] W. Jia, S. Dang, H. Liu et al., "Evidence of the formation mechanism of ZnO in aqueous solution," *Materials Letters*, vol. 82, pp. 99–101, 2012.

[12] P. Li, H. Liu, B. Lu, and Y. Wei, "Formation mechanism of 1D ZnO nanowhiskers in aqueous solution," *Journal of Physical Chemistry C*, vol. 114, no. 49, pp. 21132–21137, 2010.

[13] P. Li, H. Liu, F. X. Xu, and Y. Wei, "Controllable growth of ZnO nanowhiskers by a simple solution route," *Materials Chemistry and Physics*, vol. 112, no. 2, pp. 393–397, 2008.

[14] P. Li, Y. Wei, H. Liu, and X. Wang, "A simple low-temperature growth of ZnO nanowhiskers directly from aqueous solution containing Zn(OH)42-ions," *Chemical Communications*, no. 24, pp. 2856–2857, 2004.

[15] R. A. McBride, J. M. Kelly, and D. E. McCormack, "Growth of well-defined ZnO microparticles by hydroxide ion hydrolysis of zinc salts," *Journal of Materials Chemistry*, vol. 13, no. 5, pp. 1196–1201, 2003.

[16] N. J. Nicholas, G. V. Franks, and W. A. Ducker, "The mechanism for hydrothermal growth of zinc oxide," *CrystEngComm*, vol. 14, no. 4, pp. 1232–1240, 2012.

[17] M. Wang, Y. Zhou, Y. Zhang, S. H. Hahn, and E. J. Kim, "From $Zn(OH)_2$ to ZnO: a study on the mechanism of phase transformation," *CrystEngComm*, vol. 13, no. 20, pp. 6024–6026, 2011.

[18] J. Xie, P. Li, Y. Li, Y. Wang, and Y. Wei, "Morphology control of ZnO particles via aqueous solution route at low temperature," *Materials Chemistry and Physics*, vol. 114, no. 2-3, pp. 943–947, 2009.

[19] J. Xie, P. Li, Y. Wang, and Y. Wei, "Synthesis of ZnO whiskers with different aspect ratios by a facile solution route," *Physica Status Solidi A*, vol. 205, no. 7, pp. 1560–1565, 2008.

[20] H. Sun, "Compass: an ab initio force-field optimized for condensed-phase applications—overview with details on alkane and benzene compounds," *Journal of Physical Chemistry B*, vol. 102, no. 38, pp. 7338–7364, 1998.

[21] S. Nosé, "A unified formulation of the constant temperature molecular dynamics methods," *The Journal of Chemical Physics*, vol. 81, no. 1, pp. 511–519, 1984.

[22] Z. R. Tian, J. A. Voigt, J. Liu et al., "Complex and oriented ZnO nanostructures," *Nature Materials*, vol. 2, no. 12, pp. 821–826, 2003.

[23] J. Joo, B. Y. Chow, M. Prakash, E. S. Boyden, and J. M. Jacobson, "Face-selective electrostatic control of hydrothermal zinc oxide nanowire synthesis," *Nature Materials*, vol. 10, no. 8, pp. 596–601, 2011.